Self-reconfiguration simulations of turbines to reduce uneven farm degradation

Sam Brooks [a,*], Minhal Mahmood [a], Rajkumar Roy [a], Marinos Manolesos [a], Konstantinos Salonitis [b]

[a] *School of Science & Technology, City, University of London, Northampton Square, London, EC1V 0HB, UK*
[b] *Manufacturing and Materials Department, Cranfield University, Cranfield, MK10 7GT, UK*

A B S T R A C T

This study explored the concept of a floating offshore wind farm (FOWF) that self-reconfigures wind turbine (WT) positions. The self-reconfiguration (SR) mechanism moves degraded turbines to different farm positions to delay failures occurring and reduce power loss. A 40-turbine agent-based simulation was created utilising wind and turbine performance data. For the first time, the SR mechanism was designed and optimised with principles of self-engineering complexity. The paper demonstrates the effectiveness of the SR mechanism through an agent-based simulation approach. The optimised SR was used in FOWF simulations of 50 years of operation; SR balanced fatigue across the FOWF and led to an increased income of £5–40M at years 27–33 of operation; however, outside of these years, there is no net positive income, and by year 50 SR has cost the FOWF £4–7M more in movement costs. Lastly, simulations with repair and maintenance restricted to 10 months or less were conducted. SR delayed turbine failures, so they occurred in months when repair could be conducted. The SR reduced power loss and increased net income by up to £20M, indicating that SR could be useful when repair and maintenance times are limited. In the absence of significant operational data, a qualitative validation with experts confirmed the approach and the validity of the simulation model for a range of FOWF scenarios.

1. Introduction

Wind turbines (WTs) are a vital renewable energy source needed to meet 2050 net-zero targets. The UK government aims for 40 GW of wind power by 2030 [1]; Floating offshore wind farms (FOWFs) will form a significant portion, with the Crown Estate recently announcing 4 GW of capacity planned by 2035 [2]. Similarly, Europe's FOWF capacity is estimated to grow from 100 MW to 10 GW by 2030 [3]. Floating offshore wind turbines (FOWTs) are popular because they can benefit from higher wind speed, fewer constraints on location, flexible construction and installation, and lower demolition costs. However, FOWTs are often in areas of far offshore with adverse weather, making them costly to repair.

Studies have investigated the levelized cost of energy (LCoE) for floating offshore wind farms (FOWF), of which operation and maintenance (O&M) costs make up 11–38% [4–7]. The O&M costs depend on the FOWF distance from shore and a suitable port. Advances in sensing have led to new condition monitoring (CM) capabilities for key components such as gearboxes [8], generators [9] and bearings [10] which were previously a point of failure. Advanced artificial intelligence techniques can be used to automatically predict the WT health or its remaining useful life [11]. This can inform effective O&M strategies to reduce costs [12,13] such as preventative [14] or predictive maintenance.

WT power de-rating (reducing blade pitch and power) and wake steering (changing the yaw of the nacelle) have both been investigated extensively to reduce fatigue and increase power loss from wakes during operation [15–18]. A control to de-rate turbines in a FOWF was successfully designed to reduce fatigue on upwind turbines in Ref. [19]. Zhao et al. balanced the degradation of WTs in a fixed wind farm (WF) simulation [15,20]; upwind WTs coordinated with downwind WTs to de-rate themselves and balance fatigue and power production across the farm. Fatigue and loading reduction were achieved at the expense of power production.

Rodrigues et al. performed initial simulations into automated repositioning of FOWTs held with three moorings. Turbines were moved

---

* Corresponding author.
  E-mail address: dr.s.brooks@hotmail.com (S. Brooks).

using an active system of winches to tighten and loosen mooring lines until a position with minimal wake loss was found [20]. Han et al. conducted similar investigations but utilised a passive movement driven by aerodynamic forces on WTs to drive repositioning [21]. Few changes to current semi-submersible FOWT designs would be needed to use this movement mechanism, except longer cables and new anchorage positions [22,23]. More recent research has investigated feed-forward controllers [24] and neural network use [25] to improve this passive repositioning control. Efficiency improvements of 20%–53.5% for FOWFs are seen compared to non-optimised starting layouts. This benefit will be reduced compared to optimised FOWF layouts [26]. Extra cost of moving FOWTs and changing wind direction are also not fully considered and should be accounted for in future studies.

Brooks and Roy proposed a self-engineering (SE) system, a built-in capability to automatically register degradation and respond to repair or delay degradation and failures [27]. Examples of SE systems include self-healing materials [28], self-repairing electronics [29] and self-reconfiguring manufacturing systems [30]. This study investigated the design and simulation of a SE self-reconfiguring (SR) mechanism for a FOWF. The mechanism responds to WT degradation registered by CM and alters the WT's use to delay failures or degradation by moving degraded WTs to areas where less power is produced, extending WT life. The study investigated if SR repositioning can balance fatigue and impact power production and farm operation.

Section 2 outlines the agent-based model and data used. Indicators of fatigue and turbulence are used throughout the farm life for each WT. In Section 3, the key aspects of redundancy, repeatability and self-control (from SE complexity studies) used in SR design are optimised. Section 4 uses the optimised design in extended simulations of 50 years. Net income for WF with and without SR is calculated every year. Finally, section 5 shows the impact of using SR when restricting the number of available repair months.

2. Method

An agent-based model was constructed using AnyLogic to simulate the FOWF behaviour with and without SR. AnyLogic was used because it utilises packages on repair and maintenance and transport logistics, which can be applied to model SR movements; it also enables the integration of discrete events and stochastic features in the agent-based model. The Hywind farm in Scotland (Peterhead, Scotland) and 6 MW SWT-6.0-154 were modelled because it is a well-advanced FOWT trial with open access to site information and data [31]. Previous academic studies, available data and informal discussions with industry stakeholders were used. All results reported were averages of ten simulation runs. Error bars correspond to one standard deviation in results. An overview of the WT model is shown in Fig. 1.

2.1. Turbine layout

Only five turbines are installed at Hywind Scotland currently. Therefore, an optimised offshore WF (OWF) layout designed to minimise wake losses was taken from Amaral and Castro [32] and used with 40 FOWT. Turbines of diameter (D_T) 156m were placed at $9D_T$ towards the prevailing wind direction and $4.5D_T$ perpendicular to the prevailing wind direction. The layout between turbines is shown in Fig. 2 with a compass showing the farm angle (240° from true north). The FOWF was set 50 km from shore, where a maintenance hub was located. Each turbine was assumed to have a wireless communication link to neighbouring turbines, shown in blue Fig. 2.

2.2. Power calculation and wake effect

WT operation creates turbulence, impacting the downwind wind speed (the wake effect). An estimate for the wake effect on local wind speed (v_i) for each turbine was found using Equation (1) (from the Jensen wake model [33]). The wake effect reduces wind speed directly behind a turbine; however, as distance x from the upstream WTs increases, wind speed ($v(x)$) will approach freestream speed (V_o); Fig. 3 shows two WTs and their wakes. C_{Thrust} represents the thrust coefficient [34]. The wake diameter at distance x (D(x)) is found from $D(x) = D_T + 2kx$, where k is the wake decay coefficient (0.05 from Ref. [35]).
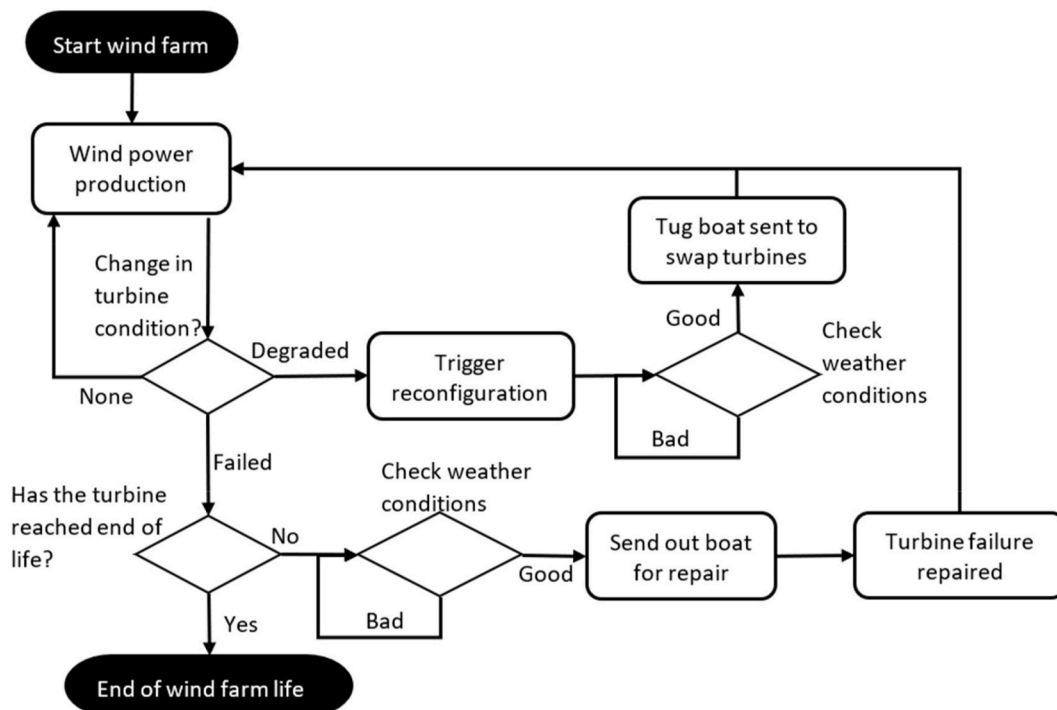

Fig. 1. – Overview flow chart of model used for the WF and WT. See supplementary material for a detailed diagram.
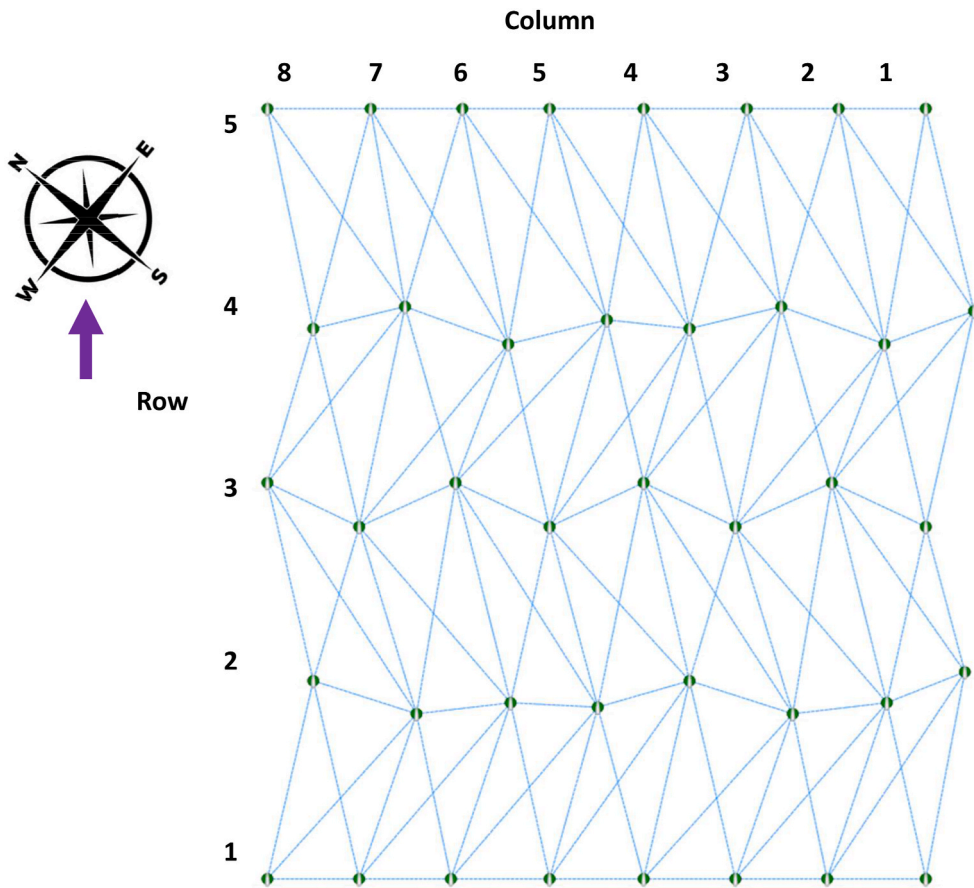
Column

Fig. 2. - Optimised WF layout used; turbine positions are green along with communication connections between turbines in blue. Top left shows a compass with a purple arrow showing the prevailing wind.
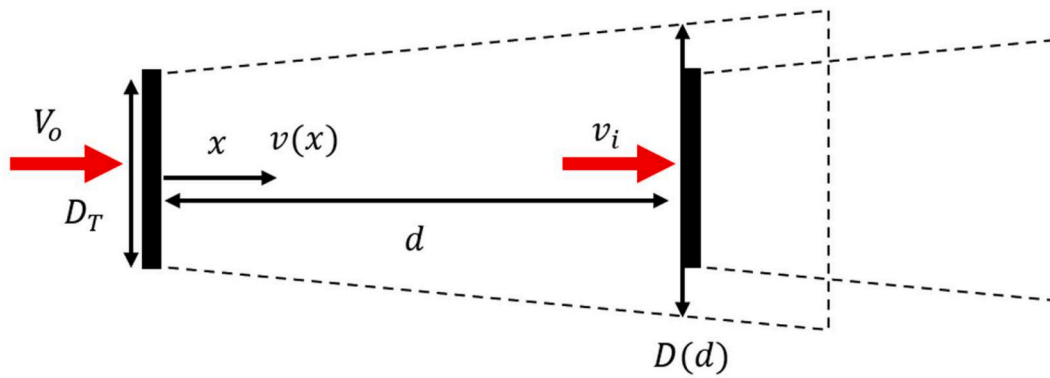

Fig. 3. – Diagram of the wake effect caused by a turbine and the parameters used.

$$1 - \frac{v_i}{V_o} = \left(1 - \sqrt{1 - C_{Trust}}\right)\left(\frac{D_T^2}{D(d)^2}\right) \tag{1}$$

Each model WT agent had a wake region which moves as the WT rotates. Wind speed was recalculated if a downwind WT fell into this wake region. When multiple wakes interact, the sum of squares method was used to find wind speed [35], shown in Equation (2).

$$\left(1 - \frac{v_i}{v_o}\right)^2 = \sum_{j}^{K}\left(1 - \frac{v_{ji}}{v_j}\right)^2 \tag{2}$$

Where K is the number of upwind turbine wakes impacting WT i; v_{ji} denotes wind speed at turbine i due to the single wake from turbine j.

Factors $1 - \frac{v_{ji}}{v_j}$ were found using Equation (1). As wind direction and speed changed, new wakes were created, and local wind speed was recalculated. This method only approximates the wake effect but is suitable for this model, where the focus is SR.

2.3. Wind data and direction

A year of hourly average wind speed and directions were taken from the UK Centre for Environmental Data Analysis [36] and their nearest monitoring site to Hywind Scotland. The data for 2021 is displayed in Fig. 4.

The most common (mode) wind direction and mean wind speed for each day were used in simulations. The wind speed and direction of this
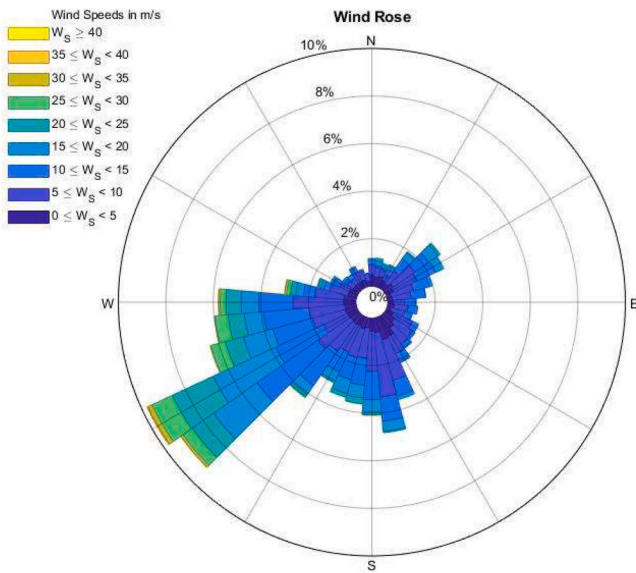
Fig. 4. - Wind rose for Peterhead Harbour over 2021.

model were updated for the correct day of the year.

2.4. Modelling fatigue degradation

Turbine power production is assumed to relate to higher wear on components such as gearboxes, generators and bearings. Turbine use and failure rate are shown to be proportional to the wind speed experienced by a turbine [37]. This study utilised the concept of a Fatigue Coefficient ($C_{fatigue}$), adapted from previous studies [15,38]. Equation (3) shows $C_{fatigue}$ calculated using power produced at the site's average wind speed ($P_{average}$) instead of the rated turbine power (as in Refs. [15, 38]); therefore, $C_{fatigue} = 1$ will occur closer to the end of design life ($T_{lifetime}$) of 20 years (175200 h).

$$C_{fatigue} = \frac{\int_{0}^{t_0} P(t) \ dt}{P_{average} T_{lifetime}} \tag{3}$$

$C_{fatigue}$ is dependent on power produced ($P(t)$) at each simulation hourly time step (t) based on the power curve [39], up to the current time step (t_o).

Studies have identified failure rates (λ) for OWTs [40], but only estimates exist for FOWT [41,42]. Mean time to failure (MTTF) is related to λ by Equation (4).

$$MTTF = \frac{1}{\lambda} \tag{4}$$

The value of $C_{fatigue}$ was linked to MTTF to create a set $C_{fatigue}$ value at which failure occurs. A fatigue coefficient threshold (C_T) was used, as shown in Equation (5) for the first threshold value ($C_T(1)$).

$$(1) = \frac{P_{average} \ MTTF}{P_{average} T_{lifetime}} = \frac{MTTF}{T_{lifetime}} \tag{5}$$

Table 1 shows the original average failure rates (λ_0), MTTF and C_T for each failure type. This failure data was used because it categorised failures in Minor, Major and Major replacement (MR) types [40], used later in SR design optimisation. However, the data does not include mooring line failures or floating foundation failures.

The threshold was repeated across turbine life at intervals. Values of C_T for each failure type ($C_{T,type}$) is defined by Equation (6) where n_{type} was the number of failures that occurred of each type. A random normally distributed value Z ($N \sim (1, 0.25^2)$) was used to add a stochastic element to each C_T.

$$C_T(n) = (n + 1 + Z) \frac{\frac{1}{\lambda_0}}{T_{lifetime}} \tag{6}$$

A value R for remaining useful life before the next failure was calculated using Equation (7).

$$R = \frac{C_T(n) - C_{fatigue}}{C_T(n) - C_T(n - 1)} \tag{7}$$

It was assumed that a smart condition monitoring system [43] on board turbines could indicate when a component had degraded and was close to R = 0.3. This threshold is based on well-monitored and studied components such as bearings and gearboxes, which can be predicted twelve to six months in advance [44,45].

Values of λ will not be constant across WT life but follow a bathtub curve. No increase in failure rate was used at the start because there was assumed to be a commissioning phase before the WF was fully operational, where initial faults would be identified. However, the function in Equation (8) was used to represent changing failure rate towards WT end of life (EOL).

$$\lambda(C_{fatigue}) = \begin{cases} \lambda_0 & C_{fatigue} < 0.5 \\ \left(1 + \beta \left(C_{fatigue} - 0.5\right)^{\beta - 1}\right) \lambda_0 & C_{fatigue} > 0.5 \\ \beta = 2.5 \end{cases} \tag{8}$$

The relationship chosen was designed to reflect an increase in O&M costs from years 11–20 compared with years 1–10 seen previously [46].

2.5. Repairing turbines

WT sent repair requests to the onshore maintenance hub (50 km away), which dispatches a repair boat for minor or major repairs or a barge for MR. The cost and length of each repair type were scaled from previous studies and summarised in Table 2.

Three restrictions on when a repair or SR can take place were modelled.

1. Wave heights were randomly generated from a Weibull distribution of the data from previous site studies [47]. Repairs and SR were paused for wave height above 1.5m, a value commonly used to limit ships' usage [48].
2. Repairs and SR movements were limited to daylight hours because operating at sea in the dark increases the risk of worker accidents or collisions between turbines and vessels, causing damage.
3. Repairs and SR were paused if the wind speed was higher than 25 m/s [41].

Table 1
- Data of λ_0, MTTF and C_T for each failure type used in simulations. Adapted from data in Ref. [40].

Failure type	λ_0 [turbine^{-1}year^{-1}]	MTTF [h]	$C_T(1)$
Minor	6.2	1436	0.00656
Major	1.1	7964	0.03640
MR	0.3	29200	0.13330

Table 2
- Average cost and length of repair for failure types used in simulations. Data from Ref. [40].

Failure	Repair cost [£]	Repair time [h]
Minor	1500	6.67
Major	69000	17.64
Major replacement	50200	116.19

2.6. Modelling turbulent loading degradation

Wake effects impact power produced by a turbine and the cyclic loading. Effective Turbulence Intensity (I_{eff}) experienced by a WT indicates fatigue loading experienced; see Equation (9).

$$= \frac{\sigma_{eff}}{V_o} \tag{9}$$

Where σ_{eff} represents the effective turbulence standard deviation. Large variations in local wind speed create higher cyclic loading. This type of loading impacts load-bearing components such as towers, blades, or joints.

Turbulence Loading Coefficient (C_{Turb}) [38] experienced by the turbine represents an estimate of the lifetime loading on a turbine, as shown in Equation (10).

$$C_{Turb} = \frac{\int_0^{t_0} I_{eff} \; dt}{T_{lifetime}} \tag{10}$$

Turbulence intensity changed depending on the distances between turbines creating wakes. Values of σ_{eff} were approximated using the ambient turbulence standard deviation (σ_v) and the difference in standard deviation induced by wakes ($\Delta\sigma_v$). Equation (11) or 12 (from Refs. [49,50]) were used depending on the minimum distance between turbines.

$$\sigma_{eff}^2 = \sigma_v^2 + \sum_{i=1}^{K} \Delta\sigma_{v,i}^2 \quad \min(x) < 10D \tag{11}$$

$$\Delta\sigma_v = \frac{1}{1.5 + \left(\frac{0.8x}{C_{Trust}D_T}\right)}$$

$$\sigma_{eff} = \sigma_v \quad \min(x) > 10D \tag{12}$$

Values for σ_v was calculated using data on ambient wind conditions from Ref. [51] $\Delta\sigma_v$ was calculated for each wake a turbine was in.

2.7. Self-reconfiguration (SR) mechanism

The SR mechanism used maned tugs to move FOWT (similar to FOWT installation), meaning SR was not automated as required for SE. A crewed tug would also probably be used initially as automated ships have not been developed. Future SR systems could utilise an autonomous boat to make a complete SE system.

The SR mechanism implemented occurs when WTs enter major or MR degradation states, as displayed in Fig. 5. SR initially occurred at two set points shown in Fig. 5.

No movement occurs for minor degradation because this would be too frequent and costly. The frequency of SR was investigated and optimised in Section 3.

Previous studies moving FOWT constrained movement to a set region, such as between three anchors [21,23,52]. This study used a novel method; each turbine could be detached and swapped to another anchorage within the farm. When a turbine is degraded, it is moved to a location where less power is produced, slowing the increase in $C_{fatigue}$ and degradation. A simple example is shown in Fig. 6 a) and b); turbine 5 degrades and is swapped with one downwind. After a repair (Fig. 6 c),
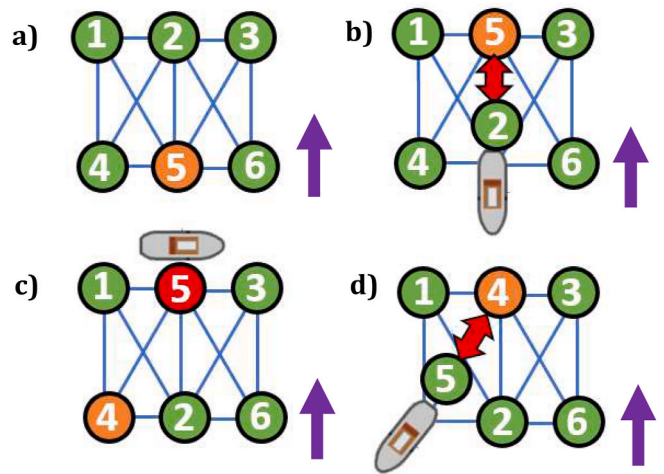
Fig. 6. – Purple arrows show wind direction; red arrows show swapping of turbines. Green circle turbines indicate 'normal operation', orange shows degraded and red circles show failed. a) shows the starting positions and b) the swap between 5 and 2. c) shows 5 failing and being repaired. d) after repair of 5 it is swapped with 4.
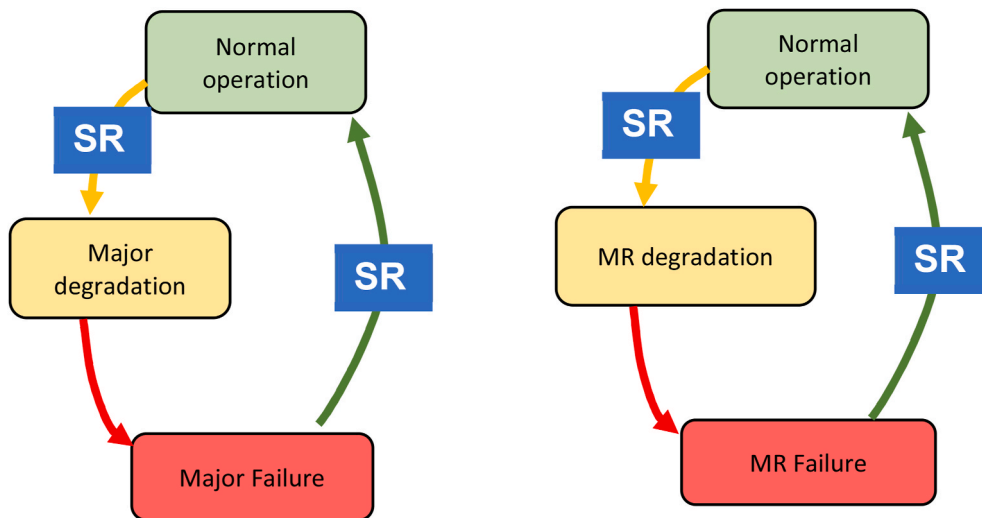

Fig. 5. Diagram of the different states for a major and MR failure. Blue boxes show all the points at which SR can occur.

1) when a turbine was registered as degraded before a major or MR failure
2) after a turbine was repaired.

the controller looks for another turbine in a worse state to swap with; an example is shown in Fig. 6 d) where turbine 5 swaps with 4, which has degraded.

The SR method and results of the study are applicable to other FOWF such as semi-submersible or barge foundations because these allow foundation movement and can be towed into position. However, current designs would need adaptions to allow anchor cables detached and attached when needed. Tension leg foundations FOWT would not work because they require a fixed tension in anchor cables and are attached well below the surface.

2.8. Cost indicators for SR

A set of cost indicators calculated if reconfiguration was potentially beneficial for the farm; this included three factors.

a. $CI_{movement}(x_1,y_1,x_2,y_2) =$ Cost of swapping turbine at position 1 with position 2
b. $CI_{PowerLoss}(x_1,y_1,x_2,y_2) =$ Indicator of difference in income lost from power loss in locations 1 and 2.
c. $CI_{repairDiff} =$ Indicator for the cost of repair or total turbine replacement once it occurs.

It is important to note that values are not real costs and are just calculated to compare the value of different actions. SR movement was beneficial when $CI_{movement} < CI_{repairDiff} + CI_{PowerLoss}$. The optimum SR was the swap of turbines that maximised X; see Equation (13). X must be positive for an SR to occur.

$$X = CI_{repairDiff} + CI_{PowerLoss} - CI_{movement} \qquad (13)$$

2.8.1. Cost indicators of movement

Previous studies have not considered the cost of movement when using moving FOWTs. This study focused on the movement cost of SR, though there will also be increased design and manufacturing costs from SR; however, these are harder to predict without detailed designs. The cost of a tug moving FOWTs at sea was calculated using information from previous installation transportation studies [41]. Table 3 shows data used for cost calculations.

Simulations recorded tug use and cost. Disconnection and reconnection of FOWT were assumed to be 4 h each. $CI_{movement}$ for individual movement is found with Equation (14). The cost of SR is found by summing the costs of all completed moves also from Equation (14).

$$CI_{Movement} = C_{fuel}\left(\left(\frac{2\,F_1 D_{move}}{1.852\,\nu}\right) + \left(\frac{2\,F_0 D_{shore}}{1.852\,\nu}\right)\right) + \Omega_2 + (\Omega_1 + \Omega_3) * M_{days} \qquad (14)$$

Distance between turbines is D_{move} and the total number of days a boat operates is M_{days}.

2.8.2. Cost indicators for repairing

The cost of repairing a turbine only occurs with a failure. Remaining useful life (R) was used to indicate the cost of replacing the par; the closer to the end of life, the higher the CI gets. Repair cost indicator

Table 3
- Information from Refs. [41,53] used for the tug cost estimate.

Variable	Value used	Nomenclature
Fuel Consumption – no turbine [l/h]	1046	F_0
Fuel Consumption – one turbine [l/h]	1942	F_1
Movement speed [knots]	10	ν
Day rate [£/day]	18735	Ω_1
Mobilisation cost [£]	3000	Ω_2
Crew cost [£/day]	220	Ω_3
Fuel cost as of May 2022 [£/l]	1.37	C_{fuel}
Distance to shore [km]	50	D_{shore}

(CI_{rep}) was approximated using Equation (15), where $Cost_r$ is the cost of repairing a failure type, taken from Table 2.

$$CI_{rep} = (1 - R)Cost_r \qquad (15)$$

Equation (16) shows the difference in potential repair cost at R of two turbines.

$$CI_{rD} = (R_2 - R_1)Cost_r \qquad (16)$$

CI for Major failure ($CI_{rD,Major}$), MR failure ($CI_{rD,MR}$) or complete turbine replacement ($CI_{rD,Turb}$) a was combined in Equation (17).

$$CI_{repairDiff} = {}_{(R_{2,Major} - R_{1,Major})Cost_{r,Major}} + (R_{2,MR} - R_{1,MR})Cost_{r,MR} + (R_{2,Turb} - R_{1,Turb})Cost_{r,Turb} \qquad (17)$$

2.8.3. Cost indicators for power lost (cost of lost opportunity)

A failed turbine no longer produces power; the total loss depends on the time needed to repair the turbine and its WF position. A turbine in the WF centre produces less power than one towards the prevailing wind edge. This difference in power loss ($CI_{PowerLoss}$) was quantified by the difference in average power produced at each position ($P_{1,ave}$, $P_{2,ave}$), electricity cost per kWh (c_{kWh}) and the repair time (t_{repair}), see Equation (18).

$$CI_{PowerLoss} = c_{kWh} t_{repair} (P_{1,ave} - P_{2,ave}) \qquad (18)$$

The wholesale price of electricity was taken as £0.15 per kWh; however, it should be noted that recent world events demonstrate this value could increase unpredictably.

2.9. Cost calculations for a wind farm

Net income in Equation (20) (NI_{total}) of the WF during the operation was found by summing net income every year (NI_Y). All costs were converted to a present value (PV) using a discount rate (r) of 0.03.

$$CashFlow_Y = Inc_{power,Y} - (Cos\,t_{SR,Y} + Cos\,t_{Opp,Y} + Cos\,t_{Main,Y} + Cos\,t_{EOL})$$

$$NI_Y = \frac{Cashflow}{(1+r)^Y} \qquad (19)$$

$$NI_{total} = \sum_{Y=0}^{n} \frac{CashFlow_Y}{(1+r)^Y} \qquad (20)$$

Cash flow was based on income from the power produced (Inc_{power}), cost of SR ($Cos\,t_{SR,Y}$), operation cost ($Cos\,t_{Opp}$), maintenance and repair costs ($Cos\,t_{Main,Y}$), and cost at the EOL ($Cos\,t_{EOL}$). These costs are explained further in each subsection. The difference between NI_{total} for a WF with ($NI_{total,SR}$) and without SR ($NI_{total,NoSR}$) is ΔNI_{total} shown in Equation (21).

$$\Delta NI_{total} = NI_{total,SR} - NI_{total,NoSR} \qquad (21)$$

This value indicates if the use of SR increases or decreases WF's income.

2.9.1. Income from power

Income from power (Inc_{power}) was the total power produced over one year of operation. An assumed electrical efficiency ($\omega = 0.8$) and a loss factor due to WT age (α) were used; see Equation (22). The loss factor is 0 at the begging of life and reduced to 16% by EOL, as noted in previous studies of WT performance with age [54].

$$Inc_{power} = c_{kWh} * \omega * (1 - \alpha) * \sum_{0}^{8670} P(t) \qquad (22)$$

$$\alpha = 0.16\,C_{fatigue}$$

2.9.2. Operation cost(Cos t_Opp)

A fixed operation cost of £150,000 per turbine per year (from Ref. [55]) covered insurance, site inspections, training, worker wages and management costs. Costs were assumed to increase by 10% in the second half of WT life ($0.5 < C_{fatigue} < 1$) [46]. This was extended to assume a 20% for operating a WT beyond the EOL($C_{fatigue} > 1$).

2.9.3. Maintenance and repair cost(Cos t_Main,Y)

Maintenance and repair costs were dependent on the number of failures each year ($n_{Minor,Y}$, $n_{Major,Y}$ and $n_{MR,Y}$) and costs of repairing each failure that year ($Cost_{r,Minor}$, $Cost_{r,Major}$ and $Cost_{r,MR}$); see Equation (23).

$$Cos\ t_{Main,Y} = n_{Minor,Y}Cost_{r,Minor} + n_{Major,Y}Cost_{r,Major} + n_{MR,Y}Cost_{r,MR} \qquad (23)$$

2.9.4. End-of-life extra cost(Cos t_EOL)

Many OWTs are only now coming to EOL, with few decommissioned. When a WF reaches EOL, strategies include extending the life of existing turbines, repowering turbines, or decommissioning turbines [56]. Three similar WT EOL scenarios were used in this study when $C_{fatigue} = 1$.

Scenario 1 (S1) – A WT's life was extended (beyond $C_{fatigue} = 1$) as modelled in other life extension studies [57,58]. Changes to O&M costs were broken down into three additional costs. Firstly, the failure rate increased, as outlined in Section 2.4. Secondly, extra inspections of blades and structural components were needed every three years, an additional annual inspection was required, and a remaining useful life survey was needed every five years [57,59]. Lastly, one of the main components which most frequently fails was assumed to need replacing to enable the WT to keep operating; Table 4 shows the four parts with the highest failure rates (from Ref. [41]) and replacement costs.

Scenario 2 (S2) – WTs were removed at $C_{fatigue} = 1$, and decommissioned individually. A decommissioning cost of £867,000 was estimated based on previous studies [5,60]. In practice, turbines would be removed in bulk to reduce cost. This would have little effect on the power production modelled but decommissioning costs would occur in stages rather than continuously as WTs fail.

Scenario 3 (S3) – WTs were replaced by an identical turbine leading to downtime for removal, transportation and installation. The site could undergo repowering; however, the future size and WT efficiency are uncertain, and the WF would need a total restructuring. A new turbine cost (£1,240,830/MW), an installation cost (£206,417/MW), a decommissioning cost, and a stoppage of operation in neighbouring turbines was applied to the model. New turbines had no degradation in power loss, and α was reset to 0. Costs were adjusted from data in Refs. [5,60].

3. Self-engineering design optimisation

3.1. Self-engineering complexity

Previous studies investigated the complexity of self-engineering systems identifying three key factors [61].

1. *Repeatability* – The number of times a response (SR) can occur
2. *Self-control* – How the mechanism is controlled and managed

Table 4

- Four systems with the highest failure rate and replacement costs, estimated in a previous FOWF study [41].

System or component	Cost to repair/ replace (£M)	Failure rate (failures/turbine/ year)	Probability of occurring
Pitch Hydraulics	7.623	1.076	0.351
Generator	1.015	0.999	0.326
Blades	0.375	0.52	0.169
Grease, oil, and cooling fluid change	0.101	0.471	0.154

3. *Redundancy* – The quantity of redundancy used in the system for SE

Different complexity levels were tested during the design and development of previous self-engineering systems [62]. A similar investigation was conducted here using Taguchi's design of experiment method to find the best system repeatability, redundancy, and self-control. Results with and without SR are compared using ΔNI_{total}.

3.1.1. Repeatability level

High, medium and low levels of repeatability were created by changing the frequency SR occurs. Fig. 5 illustrates different SR points.

- *High Complexity* – SR occurred when a turbine reached a degraded state before an MR and major failure and after these failures were repaired.
- *Medium Complexity* – SR occurred when a turbine reached a degraded state before all MR and major failures, but not after a repair.
- *Low complexity* – SR occurred only when in a degraded state before an MR failure.

3.1.2. Self-control

- *Low complexity* - Central control: SR was managed by a central control station monitoring all WT conditions and deciding which turbine should be switched. The central control could choose any turbine in rows available to switch with, not just the closest ones, as with local control. Fig. 7 (b) presents the case of central control.
- *Medium Complexity* - Local control: each turbine managed its SR, meaning it was limited to knowledge about WTs closest to itself. Controllers were on each turbine individually, meaning lots of individual controllers interacting.
- *High complexity* - Local and central control: the local controller and central control station select optimum candidates to switch with. If the central controller's choice was twice as good ($X_{central} = 2X_{local}$) as the local controller, it replaced the local control choice.

3.1.3. Redundancy level

The redundancy level focused on the number of turbines a set turbine can swap with. The local controller searched local connected WTs, while the central controller searched whole WF rows. Fig. 7 shows an example. With a low level of redundancy, only one row or one connection was searched. The number of rows or connections increased with redundancy complexity (two connections or rows for medium and all for high complexity). The more possible turbines to swap with, the better the chance of a swap helping the WF.

3.2. Improving income

Nine simulation runs were designed using an L9 Taguchi orthogonal matrix. Settings for each simulation are shown in Table 5. The aim was to improve the NI_{total}, at 30 years of operation. From the data, signal-to-noise ratios (η) were calculated using the larger-is-better approach [63]. Values for η were averaged (η_{mean}) for each setting and plotted in Fig. 8; results with higher η_{mean} are the optimum complexity levels to maximise farm NI.

In Fig. 8, a similar pattern of results is shown for all scenarios; the optimum design settings for SR were.

1. Low repeatability – SR should only be triggered for a degraded state before an MR. More frequent triggers increased the overall movement cost and lowered NI_{total}. Range and rank in Table 6 also show this was the most important factor with the largest influence on NI_{total}.
2. High redundancy – When all turbines were available to swap with, the SR controller had more options to find an optimum swap. The increase in performance between one and two rows is greater than
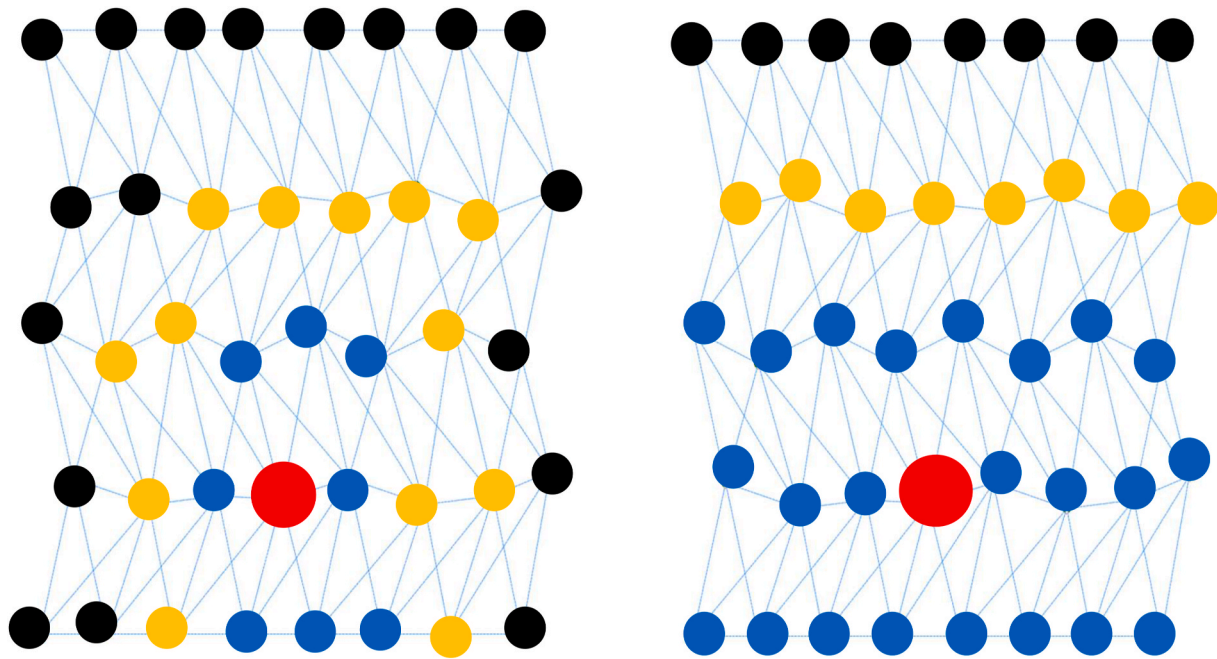
Fig. 7. Different connections for different levels of redundancy. Diagram a) shows local self-control connections and b) shows central self-control connections for a set turbine in red. Blue shows low redundancy (1 connection), yellow medium redundancy (2 connections) and black high redundancy (all connected).

Table 5
– Conditions for each level of complexity for each experiment run.

	Redundancy	Repeatability	Self-control
1	One connection/rows	MR	Local
2	One connection/rows	M and MR	Central
3	One connection/rows	M, MR and after repaired	Local and central
4	Two connections/rows	MR	Central
5	Two connections/rows	M and MR	Local and central
6	Two connections/rows	M, MR and after repaired	Local
7	All connections/rows	MR	Local and central
8	All connections/rows	M and MR	Local
9	All connections/rows	M, MR and after repaired	Central

between two and all (see Fig. 8 b). This could be because using all rows causes longer movement distances and higher fuel costs. Alternatively, it could be because two rows of access are enough to connect the outer and middle turbines where the largest differences in fatigue are seen. Ranks in Table 6 show that for S1 and S2, redundancy was the least important factor.

3. Low (central) self-control – The central controller performed better than the local one; because it gives access to whole rows of turbines, not just neighbouring ones. This was probably more noticeable at farm edges or corners because WTs had fewer WTs nearby. Behaviours appear non-linear in Fig. 8 c) because of the distinct local and central control difference. For high self-control, the mix of local and central performs better than local because it occasionally utilises the central controller but not entirely. With all WTs connected (high redundancy), there was unlikely much difference between the controllers. In practice, a central controller will be easier to manage because having multiple local controllers on WTs could lead to complex, unpredictable interactions.

3.3. Initial results

Simulations were run for 30 years to test the effect of optimised SR on FOWF. The results are shown in Table 7. The success of the SR in balancing the fatigue was indicated by the term $\Delta C_{fatigue}$, found using Equation (24).

$$\Delta C_{fatigue} = Max(C_{fatigue}) - Min(C_{fatigue}) \tag{24}$$

The results in Table 7 show that using the optimised SR settings produces a gain in income for all scenarios at 30 years. The difference is significant enough to be higher than the deviation within simulations. The $\Delta C_{fatigue}$ was reduced from 0.316 to 0.124 by using SR, showing $C_{fatigue}$ is balanced. A similar reduction was seen for ΔC_{turb} with SR.

A second optimisation, shown in supplementary material, was performed to reduce $\Delta C_{fatigue}$; however, optimisation required high repeatability with many SR movements, reducing NI_{total}. Therefore, it was not used in further experiments.

The $\Delta C_{fatigue}$ and ΔC_{Turb} only show the difference between maximum and minimum values, a more in-depth look was needed to see individual turbines. Values of $C_{fatigue}$ and C_{Turb} for turbines after 30 years are shown in Figs. 9 and 10 for one simulation. Row and column numbers refer to the original positions in Fig. 2. When no SR was used, there was a clear peak in $C_{fatigue}$ of turbines toward the prevailing wind (shown by purple arrows in Figs. 9 and 10) and higher C_{Turb} results in the WF centre. Front turbines could suffer from quicker degradation of rotational components, while middle WTs may have more damaged blades or structural components from repeated loading. The distribution of $C_{fatigue}$ is similar to those presented by previous authors looking at failure rates in WT [64]. There are some high peaks with four WT nearly at $C_{fatigue} > 1$ in Fig. 9 b. Each simulation with SR took an average of 24.8 s, while without SR was faster at 23.8 s.

3.4. Discussion

Brooks and Roy [62] previously used Taguchi's design of experiments to optimise the complexity of a self-cleaning system. High redundancy was the only similar optimised setting; higher self-control and medium repeatability in Ref. [62] differed from settings in this study. This demonstrates that different self-control or repeatability levels will be seen for different SE systems. The optimised settings are likely to be heavily influenced by cost assumptions, especially movement cost. Optimum $\Delta C_{fatigue}$ and NI_{total} cannot both be achieved. Settings from the optimisation were used in further simulations because they reduced $\Delta C_{fatigue}$ and ΔC_{Turb} compared to no SR and maximised
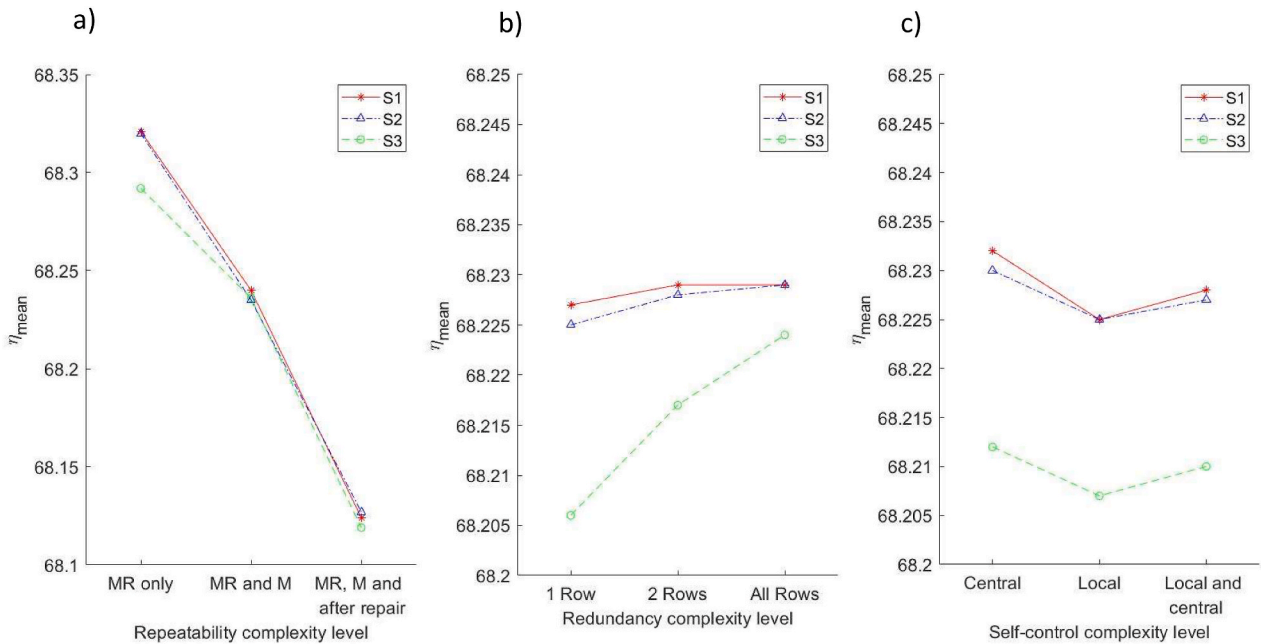
Fig. 8. Graphs showing the η_{mean} for a) repeatability, b) redundancy, and c) self-control for optimising the NI_{total} at 30 years of operation. A different line is plotted for each EOL scenario.

Table 6
– Table of range of η_{mean} values (highest minus lowest) and the rank of importance of each factor for each scenario.

Scenario		Repeatability	Redundancy	Self-control
S1	Range	0.197	0.002	0.006
	Rank	1	3	2
S2	Range	0.193	0.004	0.005
	Rank	1	3	2
S3	Range	0.174	0.019	0.005
	Rank	1	2	3

Table 7
– Results with and without SR: low repeatability, high redundancy, and low self-control.

		No SR	With SR	Difference	+/-
NI_{total} (**£M**)	S1	2596.13	2607.28	11.16	8.65
	S2	2585.70	2605.37	19.67	7.49
	S3	2500.03	2607.66	107.63	1.85
$\Delta C_{fatigue}$ (−)		0.316	0.124	−0.192	0.02
ΔC_{turb} (−)		0.095	0.05	−0.045	0.005
Number of SR movement		0	175	1751	17

NI_{total}.

Fig. 9 a) shows that at 30 years, eight WT reached the EOL when no SR was used, while none have reached EOL with SR. This caused higher income with SR because extra costs were added at EOL. Longer simulation runs will increase WTs reaching EOL in SR WF and the costs. A further investigation was performed in section 4 to look at *NI* across an extended period.

4. Extended operation

Simulations runs showed the *NI* every year and the differences in *NI* each year. Simulations were run for 50 years to show the impact of WTs reaching EOL at different rates and times. Results were plotted in three graphs for each EOL scenario from Section 2.9.4. The first graph gives *NI* for that set year of operation; this was found as described in Section 2.9.

The second graph is the ΔNI_{total}; if farm operation was stopped at that set year, this graph shows *NI* gained or lost using SR. The final graph shows turbines that have reached $C_{fatigue} \geq 1$. Due to the extended run time, simulation time increased to 44 s with SR and 38 without SR.

4.1. S1 results

Fig. 11 shows three graphs plotted for S1. Before year 28 of operation, there was a very similar *NI* for both farms; a small fall in ΔNI_{total} was then seen because of SR cost (see Fig. 11 b). Around year 28, WTs begin to reach the EOL in the WF without SR, resulting in extra maintenance and inspection costs, leading to a positive ΔNI_{total} for the next 4–5 years up to £4–5M. However, Fig. 11 c) shows at years 32–35 that all WTs in SR farms reach the EOL together, creating a high cost and a negative NI_{total} from year 35. Overall, after 50 years, there was a small decrease to -£7M for ΔNI_{total} because of the extra cost of SR.

4.2. S2 results

Fig. 12 shows results for S2, where WTs were decommissioned. As in Fig. 11, there was a positive increase in ΔNI_{total} from year 28, but it was longer until year 37, peaking in year 33 at £20M. This higher peak was because of extra power production from turbines not decommissioned in WF with SR. However, by year 35, all WTs in with SR farm had reached EOL and been removed, while WF without SR still had WTs. At 50 years, ΔNI_{total} was also down to -£4M, less than S1 because SR costs stop when turbines are removed.

4.3. S3 results

Fig. 13 outlines results for S3, where WTs were replaced. Graphs follow a similar pattern to S1 (Fig. 11). From year 27–33, ΔNI_{total} was positive, showing that SR WF increased income. The peak ΔNI_{total} was higher because of the high cost of replacing the WTs in S3. After a turbine was replaced, there was an increase in power because the WT's α value was reset to 0. After 50 years, the ΔNI_{total} was at -£6.5M, close to that in S1.
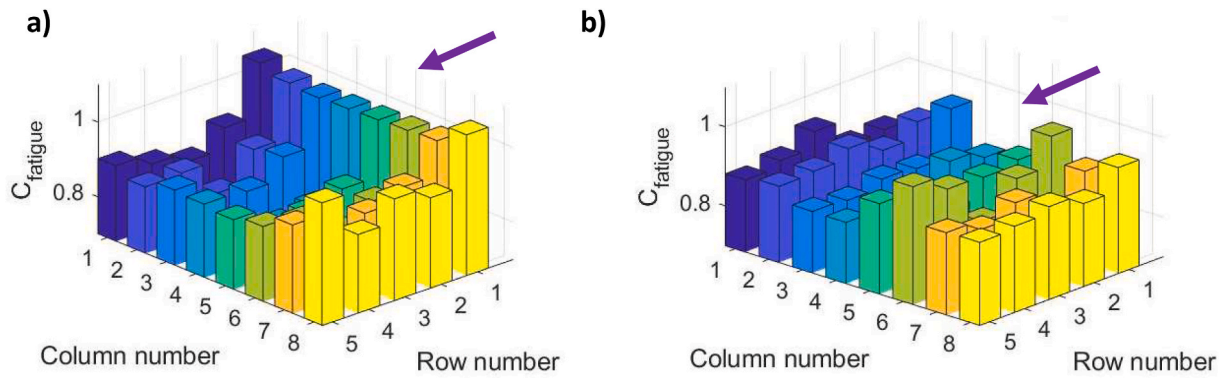
Fig. 9. Values of $C_{fatigue}$ for each turbine after 30 years. Row and column numbers are shown in Fig. 2. Graph a) is for a farm with no SR, b) is for a farm optimised for NI_{total}, and c) is optimised to reduce $\Delta C_{fatigue}$.
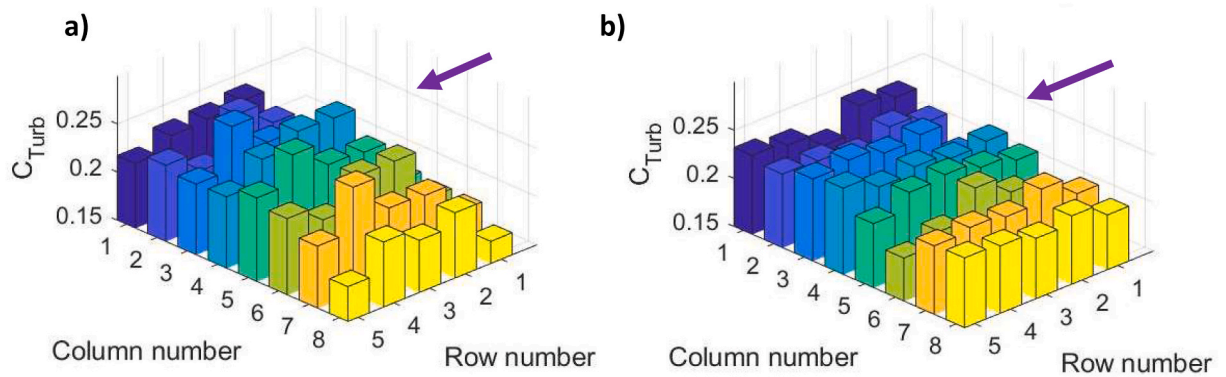

Fig. 10. Values of C_{Turb} for each turbine after 30 years. Row and column numbers are shown in Fig. 2. Graph a) is for a farm with no SR, b) is for a farm optimised for NI_{total}.
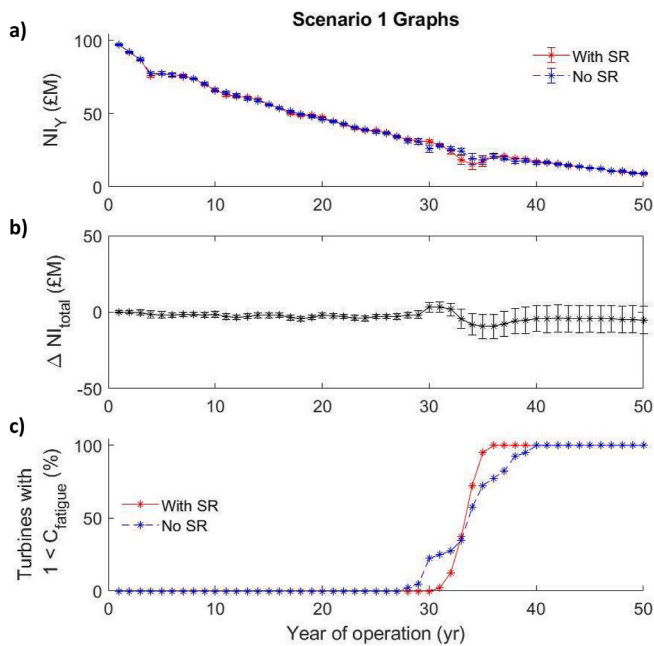

Fig. 11. Graph for S1 showing a) NI with and without SR, b) the difference in NI_{total} with and without SR, and c) the number of turbines beyond $C_{fatigue} = 1$. Data is shown at every year of operation for 50 years.
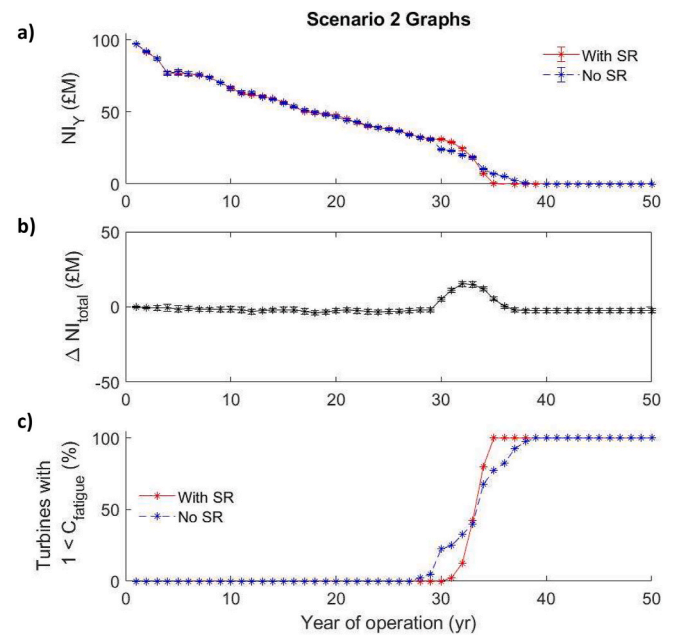
Fig. 12. Graph for S2 showing a) NI with and without SR, b) the difference in NI_{total} with and without SR, and c) the number of turbines beyond $C_{fatigue} = 1$. Data is shown at every year of operation for 50 years.

Fig. 13. Graph for S3 showing a) NI with and without SR, b) the difference in NI_{total} with and without SR, and c) the number of turbines beyond $C_{fatigue} = 1$. Data is shown at every year of operation for 50 years.
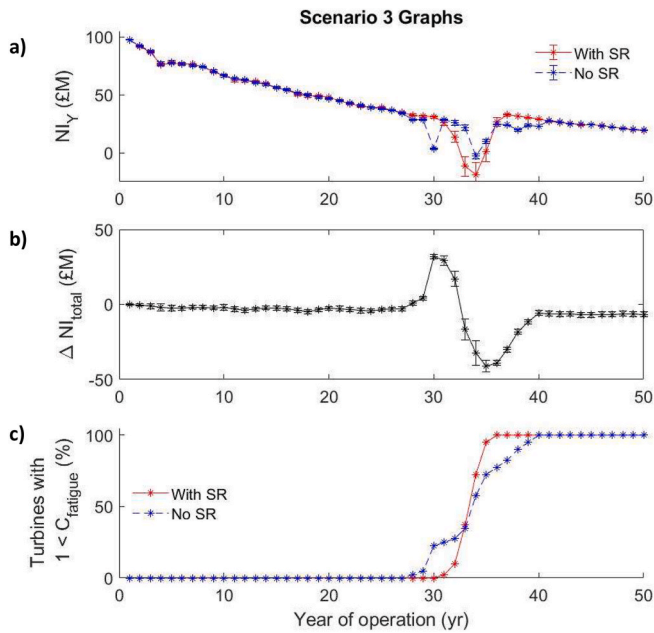
4.4. Sensitivity analysis

A sensitivity analysis was conducted on the repair cost, movement cost, operation cost, energy price, turbine spacing, failure rate, and turbines turned off during SR. Electricity price had the biggest impact on overall NI_{total} but impacted farms with and without SR equally. The number of WTs turned off during SR had the biggest impact on the ΔNI_{total} and should be investigated further in future studies. This research assumed only WTs moved need to be turned off, but if turbines in the local area $6.5\ D_T$ were turned off, SR becomes much more costly.

4.5. Discussion

Using SR has no clear benefit on total farm income for most years of operation. However, this depends on the WF EOL. A WF decommissioned between years 27 and 32 benefits financially from using SR, but not outside of this. Around year 32, 30–40% of WTs could have reached EOL in FOWFs without SR, while approximately only 10% have with SR. If decommissioning occurred when 20% of turbines reached EOL, using SR could extend farm life by 1–1.5 years. However, decommissioning when 40% or more WTs reached EOL would mean farms without SR would have a longer life. Increasing the power production or reducing design life would lead to a smaller difference in the time at which WTs with and without SR reach EOL and an even shorter period of positive ΔNI_{total}.

In all scenarios, turbines reach the EOL between years 27 and 35, later than design life, because turbine operation was stopped for high wind, maintenance or repairs.

Increased power production of WTs (with higher wind speed or efficiency) was not simulated here but would accelerate reaching $C_{fatigue} = 1$. This would move the peaks seen in Figs. 11–13 earlier and slightly higher. Although, little impact would be seen on ΔNI_{total} at 50 years.

5. Constraints on when a repair can occur

5.1. Method

A WF maintenance strategy evaluated in previous studies is to

charter vessels for repairs in set periods [65]. This could be because the farm needs a specialist in-demand vessel or because certain periods (e.g. summer months) provide more accessible days for repairs [66].

If repairs only happen in a set period (e.g. ten months of the year), failure in a non-repair month results in a wait time (t_{delay}) until the next repair window. $t_{delay}(P)$ is dependent on the rate of fatigue and power produced at a set position. Future wind speeds and power produced are unknown by WTs but were estimated using historical power produced up to the time step in the simulation. This helped predict the optimum turbine location to delay a failure if needed. The difference in power income if the turbine stays at its current position one or a new position two was given in Equation (25) for $CI_{powerLoss}$.

$$CI_{PowerLoss} = c_{kWh}(P_1(t_{delay}(P_1) + t_{repair}) - P_2(t_{delay}(P_2) + t_{repair})) \quad (25)$$

Where P_1 and P_2 were the average powers produced by turbines at 1 and 2, excluding times they were off.

5.2. Results

Simulations were run with 12 to eight months available for repairs with and without SR. Results are shown in Fig. 14 for the ΔNI_{total} over 25 years of operation.

Using SR for 25 years of farm operation led to a small decrease in NI, as shown in the previous section and Fig. 14 by the line for 12 months. A similar loss of income was seen for 11 months, indicating one month lost was insufficient to make SR beneficial. However, when constraining repairs for ten, nine or eight months, there was a positive change in income. Without SR, WT failed in the month with no repair available, leading to lost production and income. SR delays failures until a period when repairs can be made, and less power is lost.

The ΔNI_{total} does not increase with decreased number of months and instead peaks at nine months because of a limit on how long a failure can be delayed. For example, moving a degraded turbine may only delay failure by two months; this is good when nine months are available because a failure in months of no repair can be pushed to months of repair. However, this delay will not be enough for seven or eight months because a failure could be delayed but still occur in no repair months. Adjustments could be made by changing the R at which degradation and SR occur.

A peak at 22 years is seen for nine months. This is caused by larger power production with SR WF, driving a higher $C_{fatigue}$ and resulting in an increased failure rate (see section 2.4). At 22 years, this extra failure rate is beginning to reduce income for WF with SR and reduce ΔNI_{total}.
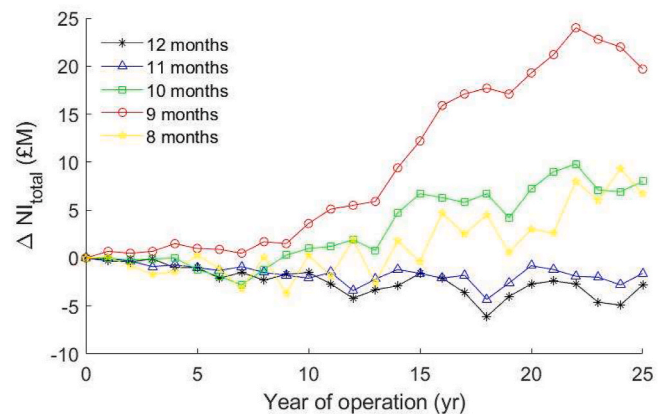

Fig. 14. Graph of ΔNI_{total} over 25 years with different numbers of months available for repair.

5.3. Discussion

The results of this section are promising, indicating SE SR could be beneficial to delay failures in set circumstances, such as supply chain disruption. If a part is unavailable or delayed, having the ability to delay the failure and maintain farm output would be useful. Another benefit could be to delay the degradation of components, so they reach EOL simultaneously, preventing multiple sperate callouts. These scenarios could be a part of future investigations into SR WFs.

6. Study validation

Lack of any significant FOWF operation data makes validation difficult. A qualitative validation approach is developed with the domain experts. The study approach, results and methods were presented to five experts in WT and FOWF with above five years of experience. Two were from academic institutions, one from a catapult, one from industry and one group of four academics (who have been classified as one respondent). Three were face-to-face semi-structured interview with a presentation, and two respondents responded in writing after reading the slides. Three key questions were asked.

1. Did the self-reconfiguration process used make sense? Are there any steps or parts missing?
2. Is the data/information needed for self-reconfiguration and the simulation realistic and available?
3. Has the data been interpreted and analysed correctly? Is there anything missing?

Experts understood the mechanism and thought the assumptions and approach were acceptable for the sector. Three of the experts were optimistic about the mechanism having a future use, and two were unsure; all Experts noted further studies would be needed when more FOWF data was available. All experts could not definitively answer question three, stating there are too many uncertainties and unknowns to say conclusively, but they commented on the validity of assumptions and methods used. Key comments made included.

4. Three participants noted a control system approach (such as blade pitching) could produce a similar effect with lower risks and easier implementation. However, as noted previously, this has been investigated [15,38].
5. Two experts noted that designing cabling and mooring for detachment and reattachment could be difficult. They also noted that mooring and floating foundation failure data should be included but acknowledged data is currently limited and based on estimates.
6. Three experts noted that the modelling method used might alter the results. A stochastic model could also help validate results. The model used here does integrate some stochastic features but is primarily a discrete event simulation.
7. Three experts agreed with question two and felt sufficient sensing existed to predict remaining life. However, two experts said there was insufficient monitoring and data for accurate assessments, noting that many failures in FOWT trials have been unexpected. This difference makes it difficult to conclude if CM is advanced enough for SR.
8. Two participants noted that wake modelling failed to consider the movement of the turbines induced by the waves. This would need detailed CFD simulations. Previous comparisons of fixed and floating foundations show only a small difference in wind speed at large separation distances (at 6D) [67]. One participant noted that SR could reduce foundation fatigue; however, there is insufficient data and studies on the long-term use of FOWF foundations to simulate this.
9. Three participants noted that more tug boats would be needed (two and four were suggested) to move the turbine because one may be deemed unsafe and have an increased risk of collision. This would increase the cost of SR by three to four times the current value.

7. Conclusion

The following bullet points outline the key paper conclusions.

- Turbines were swapped within a wind farm model to create a novel self-reconfiguration of the farm. This mechanism provides a useful way to balance the fatigue and loading across the turbines in a floating farm.
- An optimisation study used the principles of self-engineering complexity to optimise self-configuration settings for the farm income. Optimal settings included having all turbines connected, a central self-reconfiguration controller, and reconfiguring only for MR degradation.
- Farm net income with and without self-reconfiguration was compared for three end-of-life (EOL) scenarios. Self-reconfiguration delays the EOL of some WT in a farm, but subsequently, all turbines reach the EOL simultaneously rather than gradually over ten years. If a farm was decommissioned when the first turbines reach the EOL (around 27–32 years into operation), then self-reconfiguration increased net income. However, outside of this, the cost of self-reconfiguration was greater than any benefit.
- Finally, self-reconfiguration was investigated when repairs were constrained to a few months. Using self-reconfiguration increased farm income when repairs were constrained to 10 or fewer months in a year. Self-reconfiguration could be used during supply chain or maintenance disruptions which might occur by helping to slow the degradation of certain turbines. This response should be studied further.
- The study is limited by its use of only one modelling technique (agent based) and by the lack of long-term offshore failure data especially for mooring ad floating foundation components.

Data access statement

Data supporting this study are included within the article and/or supporting materials. Access at this link: click here to access.

CRediT authorship contribution statement

Sam Brooks: Conceptualization, Methodology, Investigation, Validation, Writing – original draft. **Minhal Mahmood:** Conceptualization, Methodology, Investigation. **Rajkumar Roy:** Conceptualization, Methodology, Supervision, Writing – review & editing. **Marinos Manolesos:** Writing – review & editing, Validation. **Konstantinos Salonitis:** Writing – review & editing, Validation.

Declaration of competing interest

The authors declare that they have no known competing financial interests or personal relationships that could have appeared to influence the work reported in this paper.

Data availability

Data and models can be found at this link: https://1drv.ms/u/s! AtJbRBEPiyNaarvbSEH6U1pyBFU?e=fAuZKQ

Acknowledgements

Appendix A. Supplementary data

Supplementary data to this article can be found online at https://doi.org/10.1016/j.renene.2023.02.064.

References

[1] Government Press Release, New Plans to Make UK World Leader in Green Energy, 2020.

[2] The Crown Estate, The Crown Estate Accelerates Plans for Floating Offshore Wind in the Celtic Sea with Multi-Million Pound Programme of Marine Surveys, 2022.

[3] Wind Europe, Europe Can Expect to Have 10 GW of Floating Wind by 2030, 2022.

[4] G. Rinaldi, A. Garcia-Teruel, H. Jeffrey, P.R. Thies, L. Johanning, Incorporating stochastic operation and maintenance models into the techno-economic analysis of floating offshore wind farms, Appl. Energy 301 (2021), https://doi.org/10.1016/j.apenergy.2021.117420.

[5] A. Myhr, C. Bjerkseter, A. Ågotnes, T.A. Nygaard, Levelised cost of energy for offshore floating wind turbines in a lifecycle perspective, Renew. Energy 66 (2014) 714–728, https://doi.org/10.1016/j.renene.2014.01.017.

[6] M. Lerch, M. de Prada Gil, C. Molins Borrell, G. Benveniste, Sensitivity Analysis on the Levelized Cost of Energy for, (n.d).

[7] L. Castro-Santos, A. Filgueira-Vizoso, I. Lamas-Galdo, L. Carral-Couce, Methodology to calculate the installation costs of offshore wind farms located in deep waters, J. Clean. Prod. 170 (2018) 1124–1135, https://doi.org/10.1016/j.jclepro.2017.09.219.

[8] J.P. Salameh, S. Cauet, E. Etien, A. Sakout, L. Rambault, Gearbox condition monitoring in wind turbines: a review, Mech. Syst. Signal Process. 111 (2018) 251–264, https://doi.org/10.1016/j.ymssp.2018.03.052.

[9] Z. Daneshi-Far, G.A. Capolino, H. Henao, Review of failures and condition monitoring in wind turbine generators, 2010, in: 19th International Conference on Electrical Machines, ICEM, 2010, https://doi.org/10.1109/ICELMACH.2010.5608150.

[10] Z. Liu, L. Zhang, A review of failure modes, condition monitoring and fault diagnosis methods for large-scale wind turbine bearings, Measurement 149 (2020), https://doi.org/10.1016/j.measurement.2019.107002.

[11] J. Chatterjee, N. Dethlefs, Scientometric review of artificial intelligence for operations & maintenance of wind turbines: the past, present and future, Renew. Sustain. Energy Rev. 144 (2021), 111051, https://doi.org/10.1016/j.rser.2021.111051.

[12] Z. Ren, A.S. Verma, Y. Li, J.J.E. Teuwen, Z. Jiang, Offshore wind turbine operations and maintenance: a state-of-the-art review, Renew. Sustain. Energy Rev. 144 (2021), https://doi.org/10.1016/j.rser.2021.110886.

[13] T. Elusakin, M. Shafiee, T. Adedipe, F. Dinmohammadi, A stochastic petri net model for o&m planning of floating offshore wind turbines, Energies 14 (2021), https://doi.org/10.3390/en14041134.

[14] P. Tchakoua, R. Wamkeue, M. Ouhrouche, F. Slaoui-Hasnaoui, T.A. Tameghe, G. Ekemb, Wind turbine condition monitoring: state-of-the-art review, new trends, and future challenges, Energies 7 (2014) 2595–2630, https://doi.org/10.3390/en7042595.

[15] R. Zhao, W. Shen, T. Knudsen, T. Bak, Fatigue Distribution Optimization for Offshore Wind Farms Using Intelligent Agent Control, Wind Energy, 2016, pp. 1–20, https://doi.org/10.1002/we.

[16] A. Stock, M. Cole, W. Leithead, L. Amos, Distributed control of wind farm power set points to minimise fatigue loads, 2020-July, Proc. Am. Control Conf. (2020) 4843–4848, https://doi.org/10.23919/ACC45564.2020.9147732.

[17] H. Habibi, I. Howard, S. Simani, Reliability improvement of wind turbine power generation using model-based fault detection and fault tolerant control: a review, Renew. Energy 135 (2019) 877–896, https://doi.org/10.1016/j.renene.2018.12.066.

[18] J.W. van Wingerden, P.A. Fleming, T. Göcmen, I. Eguinoa, B.M. Doekemeijer, K. Dykes, M. Lawson, E. Simley, J. King, D. Astrain, M. Iribas, C.L. Bottasso, J. Meyers, S. Raach, K. Kölle, G. Giebel, Expert elicitation on wind farm control, J Phys Conf Ser 1618 (2020), https://doi.org/10.1088/1742-6596/1618/2/022025.

[19] H. del Pozo González, J.L. Domínguez-García, Non-centralized hierarchical model predictive control strategy of floating offshore wind farms for fatigue load reduction, Renew. Energy 187 (2022) 248–256, https://doi.org/10.1016/j.renene.2022.01.046.

[20] S.F. Rodrigues, R. Teixeira Pinto, M. Soleimanzadeh, P.A.N. Bosman, P. Bauer, Wake losses optimization of offshore wind farms with moveable floating wind turbines, Energy Convers. Manag. 89 (2015) 933–941, https://doi.org/10.1016/j.enconman.2014.11.005.

[21] C. Han, J.R. Homer, R. Nagamune, Movable range and position control of an offshore wind turbine with a semi-submersible floating platform, Proc. Am. Control Conf. (2017) 1389–1394, https://doi.org/10.23919/ACC.2017.7963147.

[22] A.C. Kheirabadi, R. Nagamune, Modeling and power optimization of floating offshore wind farms with yaw and induction-based turbine repositioning, 2019-July, Proc. Am. Control Conf. (2019) 5458–5463, https://doi.org/10.23919/acc.2019.8814600.

[23] A.C. Kheirabadi, R. Nagamune, Real-time relocation of floating offshore wind turbine platforms for wind farm efficiency maximization: an assessment of feasibility and steady-state potential, Ocean Engineering 208 (2020), 107445, https://doi.org/10.1016/j.oceaneng.2020.107445.

[24] Y. Gao, A. Padmanabhan, O. Chen, A.C. Kheirabadi, R. Nagamune, A baseline repositioning controller for a floating offshore wind farm, in: Proceedings of the American Control Conference, Institute of Electrical and Electronics Engineers Inc., 2022, pp. 4224–4229, https://doi.org/10.23919/ACC53348.2022.9867574.

[25] A.C. Kheirabadi, R. Nagamune, Real-time relocation of floating offshore wind turbines for power maximization using distributed economic model predictive control, in: Proceedings of the American Control Conference, Institute of Electrical and Electronics Engineers Inc., 2021, pp. 3077–3081, https://doi.org/10.23919/ACC50511.2021.9483056.

[26] G. Froese, S.Y. Ku, A.C. Kheirabadi, R. Nagamune, Optimal layout design of floating offshore wind farms, Renew. Energy 190 (2022) 94–102, https://doi.org/10.1016/j.renene.2022.03.104.

[27] S. Brooks, R. Roy, An overview of self-engineering systems, J. Eng. Des. (2021) 1–51, https://doi.org/10.1080/09544828.2021.1914323.

[28] V.K. Thakur, M.R. Kessler, Self-healing polymer nanocomposite materials: a review, Polymer (Guildf). 69 (2015) 369–383, https://doi.org/10.1016/j.polymer.2015.04.086.

[29] A.S. Nair, P.L. Bonifus, An efficient built-in self-repair scheme for multiple RAMs, 2018-Janua, in: RTEICT 2017 - 2nd IEEE International Conference on Recent Trends in Electronics, Information and Communication Technology, Proceedings, 2018, pp. 2076–2080, https://doi.org/10.1109/RTEICT.2017.8256965.

[30] X. Li, A. Nassehi, B.I. Epureanu, Degradation-aware decision making in reconfigurable manufacturing systems, CIRP Ann. - Manuf. Technol. 68 (2019) 431–434, https://doi.org/10.1016/j.cirp.2019.04.065.

[31] O.R.E. Catapult, ORE Catapult Platform for Operational Data, 2022.

[32] L. Amaral, R. Castro, Offshore wind farm layout optimization regarding wake effects and electrical losses, Eng. Appl. Artif. Intell. 60 (2017) 26–34, https://doi.org/10.1016/j.engappai.2017.01.010.

[33] I. Katic, J. Højstrup, N.O. Jensen, A Simple Model for Cluster Efficiency, European Wind Energy Association Conference and Exhibition, 1987.

[34] T. Kunakote, N. Sabangban, S. Kumar, G.G. Tejani, N. Panagant, N. Pholdee, S. Bureerat, A.R. Yildiz, Comparative performance of twelve metaheuristics for wind farm layout optimisation, Arch. Comput. Methods Eng. 29 (2022) 717–730, https://doi.org/10.1007/s11831-021-09586-7.

[35] Z. Shao, Y. Wu, L. Li, S. Han, Y. Liu, Multiple wind turbine wakes modeling considering the faster wake recovery in overlapped wakes, Energies 12 (2019), https://doi.org/10.3390/en12040680.

[36] Met Office, MIDAS Open, UK Mean Wind Data, vol. 202107, NERC EDS Centre for Environmental Data, 2021, https://doi.org/10.5285/4d48efaaeb7f47a7963df75d6d1dbdc5.

[37] B. Hu, S. Liu, Influence of wind speed on the performance of wind turbine blades, Dongli Gongcheng Xuebao/Journal of Chinese Society of Power Engineering 36 (2016) 55–72.

[38] R. Zhao, D. Dong, C. Li, S. Liu, H. Zhang, M. Li, W. Shen, An improved power control approach for wind turbine fatigue balancing in an offshorewind farm, Energies 13 (2020), https://doi.org/10.3390/en13071549.

[39] Power Curve SWT-6.0-154, 2018. https://www.thewindpower.net/turbine_en_807_siemens_swt-6.0-154.php. (Accessed 4 May 2022).

[40] J. Carroll, A. McDonald, D. McMillan, Failure rate, repair time and unscheduled O&M cost analysis of offshore wind turbines, Wind Energy 19 (2016) 1107–1119, https://doi.org/10.1002/we.1887.

[41] G. Rinaldi, A. Garcia-Teruel, H. Jeffrey, P.R. Thies, L. Johanning, Incorporating stochastic operation and maintenance models into the techno-economic analysis of floating offshore wind farms, Appl. Energy 301 (2021), 117420, https://doi.org/10.1016/j.apenergy.2021.117420.

[42] X. Zhang, L. Sun, H. Sun, Q. Guo, X. Bai, Floating offshore wind turbine reliability analysis based on system grading and dynamic FTA, J. Wind Eng. Ind. Aerod. 154 (2016) 21–33, https://doi.org/10.1016/j.jweia.2016.04.005.

[43] R. Roy, R. Stark, K. Tracht, S. Takata, M. Mori, Continuous maintenance and the future – foundations and technological challenges, CIRP Ann. - Manuf. Technol. 65 (2016) 667–688, https://doi.org/10.1016/j.cirp.2016.06.006.

[44] Conaill Soragham, Early Fault Detection Using SCADA Data: an Exploration of E. ON's Intelligent Use of Operational Data to Identify Faults, 2016.

[45] J. Carroll, S. Koukoura, A. McDonald, A. Charalambous, S. Weiss, S. McArthur, Wind turbine gearbox failure and remaining useful life prediction using machine learning techniques, Wind Energy 22 (2019) 360–375, https://doi.org/10.1002/we.2290.

[46] I.W.E.S. Fraunhofer, Wind energy report Germany 2014, 112, http://publica.fraunhofer.de/eprints/urn_nbn_de_0011-n-354656-16.pdf, 2015.

[47] A.E. Onstad, M. Stokke, L. Sætran, Site assessment of the floating wind turbine Hywind demo, Energy Proc. 94 (2016) 409–416, https://doi.org/10.1016/j.egypro.2016.09.205.

[48] J.W. Taylor, J. Jeon, Probabilistic forecasting of wave height for offshore wind turbine maintenance, Eur. J. Oper. Res. 267 (2018) 877–890, https://doi.org/10.1016/j.ejor.2017.12.021.

[49] G.W. Qian, T. Ishihara, Wind farm power maximization through wake steering with a new multiple wake model for prediction of turbulence intensity, Energy 220 (2021), 119680, https://doi.org/10.1016/j.energy.2020.119680.

[50] A.C.P.A.S. Committee, ACP 61400-1-202x wind energy generation systems – Part 1: design requirements. https://cleanpower.org/wp-content/uploads/2021/05/ACP-61400-1-202x_Draft.pdf, 2005.

[51] Equinor and ORE Catapult, Equinor Hywind Scotland - floating wind turbine design case. https://pod.ore.catapult.org.uk/, 2019.

[52] S.F. Rodrigues, R. Teixeira Pinto, M. Soleimanzadeh, P.A.N. Bosman, P. Bauer, Wake losses optimization of offshore wind farms with moveable floating wind

turbines, Energy Convers. Manag. 89 (2015) 933–941, https://doi.org/10.1016/j.enconman.2014.11.005.

[53] Statoil, Nasdar, Hywind Scotland park - brochure. http://www.statoil.com/en/TechnologyInnovation/NewEnergy/RenewablePowerProduction/Offshore/HywindScotland/Pages/default.aspx?redirectShortUrl=http://www.statoil.com/HywindScotland, 2016.

[54] I. Staffell, R. Green, How does wind farm performance decline with age? Renew. Energy 66 (2014) 775–786, https://doi.org/10.1016/j.renene.2013.10.041.

[55] Offshore Reneable Catapult, Wind farm costs - ORE. https://guidetoanoffshorewindfarm.com/wind-farm-costs, 2020.

[56] A.M. Jadali, A. Ioannou, K. Salonitis, A. Kolios, Decommissioning vs. repowering of offshore wind farms—a techno-economic assessment, Int. J. Adv. Manuf. Technol. 112 (2021) 2519–2532, https://doi.org/10.1007/s00170-020-06349-9.

[57] L. Ziegler, E. Gonzalez, T. Rubert, U. Smolka, J.J. Melero, Lifetime extension of onshore wind turbines: a review covering Germany, Spain, Denmark, and the UK, Renew. Sustain. Energy Rev. 82 (2018) 1261–1271, https://doi.org/10.1016/j.rser.2017.09.100.

[58] L.M. Abadie, N. Goicoechea, Old wind farm life extension vs. Full repowering: a review of economic issues and a stochastic application for Spain, Energies 14 (2021), https://doi.org/10.3390/en14123678.

[59] T. Rubert, D. McMillan, P. Niewczas, A decision support tool to assist with lifetime extension of wind turbines, Renew. Energy 120 (2018) 423–433, https://doi.org/10.1016/j.renene.2017.12.064.

[60] C. Bjerkseter, A. Agotnes, Levelised Cost of Energy for Offshore Floating Wind Turbine Concepts, Norwegian University of Life Sciences, 2013.

[61] S. Brooks, R. Roy, A complexity framework for self-engineering systems, Smart Sustain Manuf Syst 4 (2020) 254–259.

[62] S. Brooks, R. Roy, Design and complexity evaluation of a self-cleaning heat exchanger, Int. J. Heat Mass Tran. 191 (2022), https://doi.org/10.1016/j.ijheatmasstransfer.2022.122725.

[63] M. Phandke, Quality Engineering Using Robust Design, Prentice Hall, Englewood Cliffs, NJ, 1989. papers2://publication/uuid/A0B29225-0CA3-46D1-B3F1-1AF9E00909F7.

[64] J. Tian, D. Zhou, C. Su, F. Blaabjerg, Z. Chen, Wake Effects on Lifetime Distribution in DFIG-Based Wind Farms, 2017 IEEE 3rd International Future Energy Electronics Conference and ECCE Asia, 2017, IFEEC - ECCE Asia, 2017, pp. 208–213, https://doi.org/10.1109/IFEEC.2017.7992444.

[65] I.A. Dinwoodie, D. McMillan, Operational strategies for offshore wind turbines to mitigate failure rate uncertainty on operational costs and revenue, IET Renew. Power Gener. 8 (2014) 359–366, https://doi.org/10.1049/iet-rpg.2013.0232.

[66] R. Martin, Sensitivity analysis of offshore wind farm operation and maintenance cost and availability, Renew. Energy 85 (2016) 1226–1236, https://doi.org/10.1016/j.renene.2015.07.078.

[67] H. Johlas, L. Martınez-Tossas, M. Lackner, D. Schmidt, M. Churchfield, Large eddy simulations of offshore wind turbine wakes for two floating platform types, in: NAWEA WindTech 2019 Journal of Physics, Conference Series, 2019.

2023-03-06

Self-reconfiguration simulations of turbines to reduce uneven farm degradation

Brooks, Sam